Diffusive Permeability and Selectivity of Nanocomposite Membranes

Reghan J. Hill*

Department of Chemical Engineering and McGill Institute for Advanced Materials, McGill University, Montreal, Quebec, Canada H3A 2B2

The permeability of certain polymer membranes with impenetrable nanoinclusions increases with the particle volume fraction (Merkel et al. *Science* **2002**, *296*, 519−522). This intriguing discovery contradicts even qualitative expectations based on Maxwell's classical theory of conduction/diffusion in composites with homogeneous phases. This paper describes a theoretical model that captures the observed dependence of the bulk permeability and selectivity on the inclusion size and volume fraction, thereby providing a straightforward connection between membrane microstructure and performance. An essential feature of the theory is a polymer-segment depletion layer at the inclusion−polymer interface. The accompanying increase in free volume leads to a significant increase in the local penetrant diffusivity, which, in turn, increases the bulk permeability and selectivity.

1. Introduction

Polymeric membranes facilitate a variety of molecular separations. Because their microstructure is of molecular scale, the polymer architecture can be tailored to specific penetrant mixtures. Merkel et al.[1,2] recently showed that incorporating nanometer-sized inorganic particulates into certain amorphous polymer glasses increases the membrane permeability and selectivity. Because of its significant technological applications, this discovery has stimulated many experimental investigations.[3−6] However, a theory that quantifies how the inclusion size and concentration affect the permeability and selectivity has yet to emerge. Indeed, Merkel et al. highlighted that classical Maxwell-like theories fail to describe even the qualitative trends. An important observation that they did make, which is pursued quantitatively in this paper, is that Cohen and Turnbull's free-volume theory[7] can be invoked to explain qualitative features of the experiments.

The principal assumption in this work is that a repulsive interaction between the inclusions and the polymer leads to an increase in the free volume at the interface. This is supported by measurements indicating that the average *polymer* density decreases with increasing silica content.[2] Also, transmission electron microscopy (TEM) images of silica-based nanocomposites reveal various degrees of particle aggregation,[2] which is indicative of an attractive interparticle potential. In this work, the attraction is assumed to arise from a depletion of polymer at the inclusion−polymer interface. Note that quiescent solutions of polymer, silica, and solvent often phase separate, and chemical surface modifications have a significant influence on dispersion stability and inclusion−polymer adhesion.[2,8] For example, the surfaces of the silica particles used in Merkel et al.'s experiments are modified to increase their hydrophobicity and, hence, improve their compatibility with the organic solvent that disperses the polymer. In this work, the solvent−polymer interaction is assumed to be strong enough to yield a repulsive interaction between the polymer chains and inclusions.

During solvent evaporation, the polymeric phase is transformed from a dilute or semidilute solution, through a concentrated solution and melt, to an amorphous glass. These steps are depicted in Figure 1. In this work, the amorphous glassy microstructure is assumed to reflect the equilibrium microstructure that prevailed while in a concentrated solution. Diffusion coefficients of high-molecular-weight polymers in semidilute solutions are in the range[9] $D \approx 10^{-11}-10^{-13}$ m^2 s^{-1}. Therefore, the characteristic time for a polymer to diffuse (reptate) a distance comparable to its size, $l \approx 10$ nm, say, will be at most $\sim l^2/D \approx 10^{-3}$ s. Cast membranes are dried over a period of about 24 h,[2] so, assuming the average polymer concentration remains uniform, chains have time to adopt equilibrium conformations. However, in the last stage of drying, which is assumed to occur at constant polymer density, with a polymer volume fraction ≈ 0.8, for example, the characteristic time for a uniform solvent front to traverse a polymer is ~ 0.1 s. Therefore, because chain mobility decreases with increasing polymer volume fraction, it is not unreasonable to expect equilibrium conformations to be *frozen* into the (final) glassy state.

For steady gas permeation across a membrane with thickness L, the diffusive flux is

$$|\langle \boldsymbol{j} \rangle| = -D^{\mathrm{e}} \Delta n / L \tag{1}$$

where D^{e} is the effective diffusivity and Δn is the differential concentration of the diffusing penetrant. In this work, the gas solubility is assumed to be independent of solids concentration, so the inclusions influence the permeability only through their role in modifying the effective diffusivity D^{e}. This should be a reasonable approximation for the polymer composites and penetrants to which the model is compared. Merkel et al. showed that the solubilities of nitrogen and methane in poly(4-methyl-2-pentyne) (PMP)/silica composites are independent of the silica loading.[2] Similar conclusions were drawn for *n*-butane. For PMP/silica composites, which form the basis of the theoretical interpretation of experiments below, Merkel et al. conclude that permeability and selectivity are enhanced principally by changes in penetrant mobility. They also presented data showing that the most significant influence on the penetrant diffusivity comes from the silica loading, not the relatively small changes due to penetrant concentration.

Merkel et al.'s experiments exhibit *reverse selectivity*, meaning that the permeability of larger molecules is enhanced more than smaller ones. They point out that this necessitates molecular-scale perturbations to the polymer microstructure, which precludes the notion that the permeability is enhanced by shells

* Corresponding author. E-mail: reghan.hill@mcgill.ca. Tel.: (514) 398-6897. Fax: (514) 398-6678.

10.1021/ie0512035 CCC: $33.50
Published on Web 03/17/2006

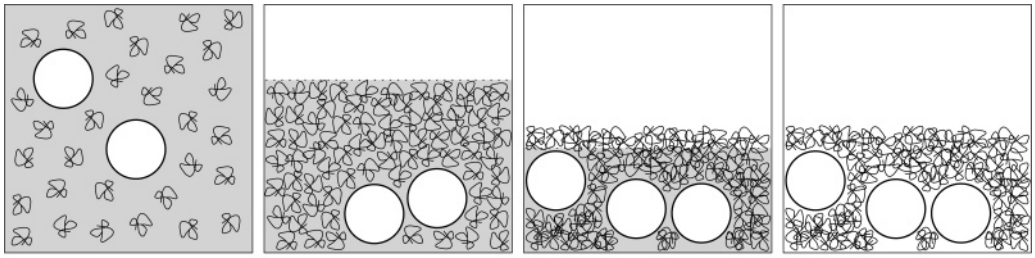

Figure 1. Schematic of the microstructural evolution during the casting of a polymeric nanocomposite membrane: (a) dilute mixture of polymer chains (filaments), solvent (grey shading), and nanoinclusions (circles); (b) solvent evaporation at uniform density leads to a semidilute polymer solution, depletion attraction between inclusions, increased bulk viscosity, and slowing chain (reptation) dynamics; (c) drying at constant density, with an amorphous glass residing behind the receding (downward) solvent front; (d) dry nanocomposite with amorphous glassy polymer. In (d), polymer chains are *frozen* in the quasi-equilibrium conformations that prevailed when saturated with solvent (c).

of void space, for example, between the (impenetrable) inclusions and surrounding polymer. Rather, a continuous change in the polymer density (free volume) is suggested.

2. Theory

In this section, the radially varying polymer segment density distribution surrounding a single inclusion in an unbounded polymer matrix is approximated using de Gennes' self-consistent mean-field theory. The varying segment density is then linked to the penetrant diffusivity using Cohen and Turnbull's free-volume theory, as proposed by Merkel et al. Finally, the penetrant concentration disturbances prevailing in a dilute, random distribution of inclusions are averaged to approximate the effective penetrant diffusivity for the composite. The microstructure that underlies this model is depicted schematically in Figure 2. Panel (a) shows a single inclusion embedded in an unbounded polymeric glass. There is a thin region close to the particle surface where polymer segments are depleted. The radial polymer segment density, whose structure is described below, is plotted in panel (b) with a representative profile of the accompanying penetrant diffusivity.

Positron annihilation lifetime spectroscopy (PALS) studies[1,2,5] reveal that high-permeability polymers have small and large free-volume elements whose radii span the range 0.3−0.60 nm. Furthermore, pulse field gradient (PFG) NMR diffusion studies[3,6] reveal heterogeneity on micron length scales, which, in turn, suggests tortuous interconnected networks of free-volume elements. When silica inclusions are incorporated, PALS indicates a significant increase in the number of large free-volume elements, with a relatively small increase in their size (∼10%), while PFG NMR points to increased connectivity of regions with an increased density of free-volume elements.

The conclusions drawn from PFG NMR and PALS are consistent with the theory presented here if the free-volume elements created by the addition of nanoparticles are accepted as residing at the particle−polymer interface. In panel (b) of Figure 2, for example, the thickness of the depleted layer is approximately $1.5\xi \approx 1.2$ nm, which is approximately twice the radius of the large free-volume elements ascertained by PALS. Therefore, the experimental and theoretical interpretations are compatible if the depleted layer is viewed as a monolayer of free-volume elements.

Note that, if the inclusions are well-dispersed, then the characteristic size of connected domains would be limited by the inclusion size $2a \approx 13$ nm. While this is considerably larger than the size of the free-volume elements, micron-sized networks (as suggested by PFG NMR) would require primary particles to aggregate, which is evident from TEM.[1,2] Because the present theory does not account for particle contacts, this shortcoming

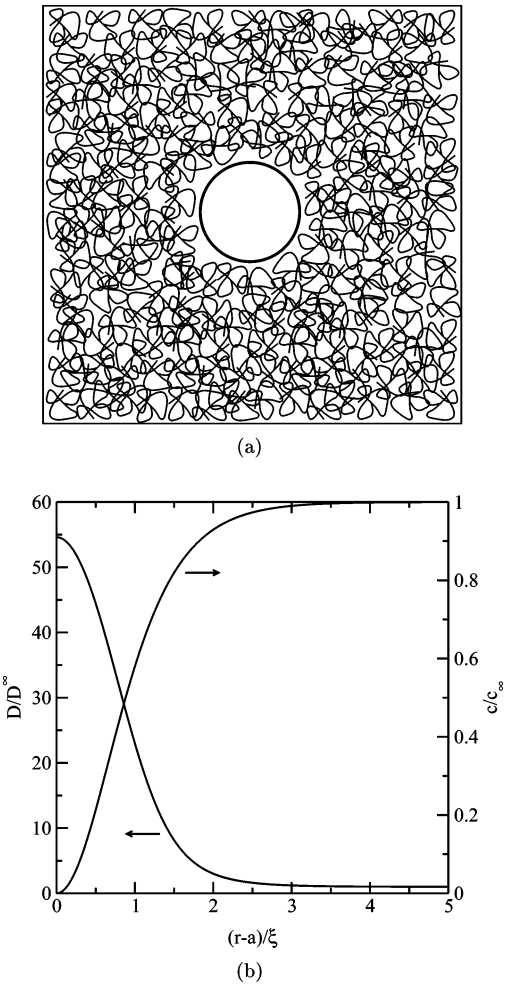

Figure 2. (a) Schematic of the microstructure that underlies the single-particle problem used in this work to calculate the dipole strength and, hence, the bulk diffusivity of small penetrant molecules in nanocomposites with small inclusion volume fractions. (b) Radially varying diffusion coefficient $D(r)/D^{\infty}$ (left axis, eq 6) and segment density $c(r)/c_{\infty}$ (right axis, eq 2) with $\phi_{\infty} = 1$, $v_m^* = 1.0$, and $\phi^* = 0.8$. The depleted layer thickness ($\approx 1.5\xi = 1.2$ nm) corresponds well with the diameter of the large free-volume elements (1.1−1.2 nm) ascertained by PALS experiments.[1,5]

is, perhaps, one of the most important limitations of the approach. Nevertheless, the model accurately describes many of the qualitative and quantitative aspects of Merkel et al.'s experiments, so it may still prove to be valuable in achieving a complete understanding of the complicated microstructure.

2.1. Polymer Segment Density Distribution. A tractable analytical expression for the radial polymer segment density is obtained from a self-consistent mean-field model, with the so-

called ground-state approximation and a flat interface.[10] The influence of curvature (finite inclusion radius) is of secondary importance and is, therefore, neglected. With a repulsive interaction between the polymer segments and the solid, the segment concentration is[10]

$$c(r) = c_\infty \tanh^2[(r - a)/\xi] + O(\xi/a) \tag{2}$$

where c_∞ is the bulk concentration and $\xi = l/\sqrt{3\upsilon c_\infty}$ is the polymer correlation length, with l being the segment length and υ being the excluded volume (per segment).

Note that the mean-field potential that underlies eq 2 is proportional to the segment density, and in this sense, it is appropriate for semidilute solutions. However, because correlations are neglected, the theory predicts the incorrect segment-concentration dependence of the correlation length.[10] For concentrated solutions and melts, screening of the excluded-volume interactions may be invoked to justify the neglect correlations. However, in this case, the mean-field potential should have a much stronger (nonlinear) dependence on the segment concentration. On the basis of these shortcomings, it must be emphasized that the primary role of eq 2 is to provide a simple (two-parameter) model that exhibits a monotonic change in the segment density over a characteristic length ξ.

References connecting ξ to υ and c_∞ below serve to establish that the parameters inferred from experiments provide an (at least) qualitative interpretation of reality. Note that the correlation length inferred by fitting the model to Merkel et al.'s experiments with silica embedded in PMP is $\xi \approx 0.8$ nm. This is of the expected order of magnitude, and because it is small compared to the inclusion radius $a \approx 6.5$ nm, the neglect of surface curvature is reasonably justified.

2.2. Local Penetrant Diffusivity. Cohen and Turnbull's statistical mechanical theory[7] yields a penetrant diffusion coefficient

$$D = A \exp(-\gamma \upsilon_m/\upsilon_f) \tag{3}$$

where A and γ are constants, υ_m is the minimum free volume required for a penetrant molecule to escape its cage of neighboring atoms and, hence, undergo diffusive migration, and υ_f is the available free volume per volume-occupying element. In this work, each atom is assumed to occupy, on average, a volume υ_0, where $\upsilon_0^{1/3}$ is of the order of a covalent bond length ($\sim$1.5 Å). By considering the total volume, which comprises the sum of free and occupied volume, it follows that

$$\upsilon_f = \upsilon_0[m_1/(\upsilon_0 n_1 \rho) - 1] \tag{4}$$

where m_1 is the mass of a monomer (repeat unit), n_1 is the number of atoms per monomer, and ρ is the (mass) density.

It is convenient to introduce a segment volume fraction $\phi = cl^3$, which, by conservation of chain contour length and mass, can be written as

$$\phi = (\rho/m_1) l_1 l^2 \tag{5}$$

where l_1 is the length of a monomer. Then, combining eqs 2−5 gives

$$D = D^\infty \exp\left[-\frac{\upsilon_m^* \phi^*(\phi - \phi_\infty)}{(1 - \phi^*\phi)(1 - \phi^*\phi_\infty)}\right] \tag{6}$$

where

$$\phi^* = n_1 \upsilon_0/(l_1 l^2) \quad \text{and } \upsilon_m^* = \gamma \upsilon_m/\upsilon_0 \tag{7}$$

are dimensionless parameters that reflect the prevailing atomic and molecular geometry.

Setting the bulk polymer volume fraction $\phi_\infty = c_\infty l^3 \approx 1$ and $\upsilon \approx l^3$, it follows that $l^2 \approx m_1/(l_1 \rho_\infty)$, $\xi \approx l/\sqrt{3}$, and

$$\phi^* \approx n_1 \upsilon_0 \rho_\infty / m_1 \tag{8}$$

where ρ_∞ is the bulk (unperturbed) polymer density. Under these conditions, $1 - \phi^*$ is the fractional free volume of the bulk polymer, and the (maximum) diffusivity at the inclusion−polymer interface becomes

$$D(r = a) \approx D^\infty \exp[\upsilon_m^* \phi^*/(1 - \phi^*)] \tag{9}$$

Clearly, the diffusivity at the interface can be much larger than that in the bulk when $\phi^* < 1$ and $\upsilon_m^* < 10$. Note that reverse selectivity prevails, because the diffusivity decreases continuously with increasing radial distance from the inclusion−polymer interface.

Consider, for example, poly(4-methyl-2-pentyne) (PMP), for which $n_1 = 15$, $m_1 = 81$ g mol^{-1}, $l_1 \approx 3$ Å, and $\rho_\infty \approx 840$ kg m^{-3}. These values[2] give $l \approx 0.73$ nm and $\xi \approx 0.42$ nm, so with[3] $1 - \phi^* = 0.22$, it follows that $\upsilon_0^{1/3} \approx 2.0$ Å and $\upsilon_f^{1/3} \approx 1.3$ Å. Note that the same values of υ_0 and υ_f emerge for poly(*p*-trimethylsilyl styrene) (PTMSS), another highly permeable glass-forming polymer.

2.3. Average Diffusivity. With a statistically homogeneous microstructure, the average diffusive flux can be expressed as a volume average

$$\langle \mathbf{j} \rangle = V^{-1} \int_V \mathbf{j}\, dV \tag{10}$$

where the integration is over the discrete and continuous phases of an elementary volume V. The local diffusive flux is (Fick's first law)

$$\mathbf{j} = -D(\phi) \nabla n \tag{11}$$

where n is the penetrant concentration. Under steady conditions, conservation demands

$$\nabla \cdot [D(\phi) \nabla n] = 0 \tag{12}$$

with a no-flux boundary condition at $r = a$, a vanishing disturbance as $r \to \infty$, and $D(r)$ from eqs 2 and 6.

When the particle volume fraction

$$\phi_p = n_p (4/3) \pi a^3 \ll 1 \tag{13}$$

the average flux is (see Appendix A)

$$\langle \mathbf{j} \rangle \approx -D^\infty \langle \nabla n \rangle + 3\phi_p (B/a^3) D^\infty \langle \nabla n \rangle + O(\phi_p^2) \tag{14}$$

where $\langle \nabla n \rangle$ is the average concentration gradient and B is the dipole strength, i.e.,

$$n \to \langle \nabla n \rangle \cdot \mathbf{r} + B \langle \nabla n \rangle \cdot \mathbf{r} r^{-3} \text{ as } r \to \infty \tag{15}$$

The (scaled) average diffusivity is

$$D^e/D^\infty = 1 - 3\phi_p (B/a^3) + O(\phi_p^2) \tag{16}$$

In this work, the penetrant flux arises from the gradient of an ideal chemical potential and, hence, the potential is independent of the polymer concentration. A slightly more sophisticated model emerges from a Nernst−Plank equation of the form

$$-\gamma(c)\mathbf{v} - kT\nabla \ln[n\psi(c)] = 0 \tag{17}$$

where $\gamma(c)$ and $\psi(c)$ are the solute friction coefficient and activity coefficient, respectively, which, in general, depend on the local polymer concentration c and, possibly, the solute concentration n. The flux $\mathbf{j} = n\mathbf{v}$ that emerges from eq 17 can be written as

$$\mathbf{j} = -D\nabla n - nD\nabla \ln \psi \tag{18}$$

where $D = kT/\gamma(c)$. Clearly, this reduces to eq 11 when ψ is independent of the polymer (and solute) concentration. Otherwise, the model precludes a uniform bulk penetrant concentration gradient. Such complications, which appear to be of secondary importance for the cases considered below, are beyond the scope of the present study and are not pursued further here.

2.4. Two-Body Interactions in a Dilute Composite. Jeffrey[11] calculated the $O(\phi_p^2)$ correction to Maxwell's well-known $O(\phi_p)$ result for homogeneous inclusions in a homogeneous continuum. Because the two-body interactions in a dilute composite are dominated by interactions between distant particles, Jeffrey's $O(\phi_p^2)$ results can be expressed in terms of the single-particle dipole strength B. Jeffrey showed that his exact calculations agree (to a reasonable approximation) with a relatively simple formula (after Hashin[11])

$$D^e/D^\infty = 1 - 3(B/a^3)\phi_p + 3(B/a^3)^2\phi_p^2[1 + 2\delta(\alpha - 1)/(\alpha + 2)] + ... \tag{19}$$

where $\alpha = D^d/D^\infty$ and $\delta \approx 0.22$; here, D^d and D^∞ are the diffusivities in the discrete and continuous phases. In the dilute limit $\phi_p \to 0$ (e.g., eq 51 with $D^s = D^\infty$), α can be expressed in terms of the dipole strength via

$$B/a^3 = (1 - \alpha)/(\alpha + 2) \tag{20}$$

It follows that

$$\alpha = (1 - 2B/a^3)/(1 + B/a^3) \tag{21}$$

and hence, eq 19 may be written as

$$D^e/D^\infty = 1 - 3(B/a^3)\phi_p + 3(B/a^3)^2(1 - 2\delta B/a^3)\phi_p^2 + ... \tag{22}$$

The $O(\phi_p^2)$ results below are calculated from eq 22 with the same dipole strength B that appears in the exact $O(\phi_p)$ theory (eq 16). In this manner, α (from eq 21) may be viewed as the (scaled) diffusivity of a homogeneous sphere that yields the same far-field disturbance as an inhomogeneous (or composite) inclusion.

2.5. Selectivity. The flux of the jth solute species across a membrane with thickness L is

$$\langle \mathbf{j}_j \rangle = -D_j^e \langle \nabla n_j \rangle \tag{23}$$

where D_j^e is the effective diffusivity and $\langle \nabla n_j \rangle$ is the average concentration gradient. Because the average concentration is not easily measured, it is convenient to write it in terms of the solute partial pressures on each side of the membrane. Accordingly,

$$\langle \nabla n_j \rangle = [n_j(L) - n_j(0)]/L = [H_j(L)p_j(L) - H_j(0)p_j(0)]/L \tag{24}$$

where H_j is Henry's coefficient and p_j is the partial pressure. Since it is only the partial pressure and membrane thickness that are readily measured, the membrane permeability is defined as

$$P_j \equiv \frac{|\langle \mathbf{j}_j \rangle| L}{|p_j(L) - p_j(0)|} = D_j^e \frac{|H_j(L)p_j(L) - H_j(0)p_j(0)|}{|p_j(L) - p_j(0)|} \tag{25}$$

This clearly shows how the permeability depends on the solubility *and* mobility of the penetrant in the membrane (via H_j and D_j^e, respectively). Note that, if Henry's coefficients are independent of pressure, which may be a reasonable approximation when pressure differentials are not too large, then

$$P_j = D_j^e H_j \tag{26}$$

The selectivity for two species, denoted 1 and 2, is defined as

$$\alpha_{12} \equiv P_1/P_2 = \frac{D_1^e}{D_2^e} \frac{|H_1(L)p_1(L) - H_1(0)p_1(0)|}{|H_2(L)p_2(L) - H_2(0)p_2(0)|} \frac{|p_2(L) - p_2(0)|}{|p_1(L) - p_1(0)|} \tag{27}$$

Again, if Henry's coefficients are independent of pressure, then

$$\alpha_{12} = (D_1^e/D_2^e)(H_1/H_2) \tag{28}$$

Since the model advanced in this work addresses only the influence of D_j^e on the permeability, let us write the selectivity as

$$\alpha_{12} = \alpha_{12}^* \frac{|H_1(L)p_1(L) - H_1(0)p_1(0)|}{|H_2(L)p_2(L) - H_2(0)p_2(0)|} \frac{|p_2(L) - p_2(0)|}{|p_1(L) - p_1(0)|} \tag{29}$$

where

$$\alpha_{12}^* = D_1^e/D_2^e \tag{30}$$

is termed the diffusivity (or mobility) selectivity. In the absence of inclusions, α_{12}^* is equal to the ratio of the bulk diffusion coefficients,

$$\alpha_{12}^* \to D_1^\infty/D_2^\infty \text{ as } \phi_p \to 0 \tag{31}$$

Below, the ratio $\alpha_{12}^*(\phi_p)/\alpha_{12}^*(0)$ is examined to highlight the role of inclusions in enhancing both the permeability and the reverse selectivity of a membrane.

3. Results

Results are presented below with $\phi_\infty = 1$ and $\phi^* = 0.8$. The two remaining independent (dimensionless) parameters are the scaled correlation length ξ/a and the scaled penetrant size $\upsilon_m^* = \gamma\upsilon_m/\upsilon_0$. Here, the principal influence of υ_m^* is to set the diffusion coefficient at the interface: $D(r = a) = D^\infty \exp(4\upsilon_m^*)$.

3.1. Permeability. As expected, all values of $\upsilon_m^* > 0$, with sufficiently large ξ/a, increase the effective diffusivity. However, if the local increase in diffusivity is not sufficiently large, or the depletion layer is insufficiently thick, the effective diffusivity

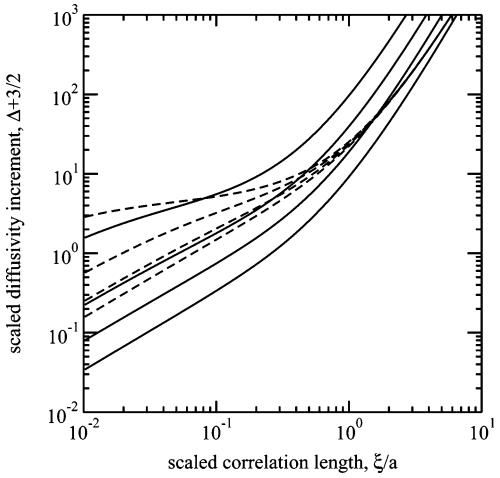

Figure 3. The scaled diffusivity increment $\Delta = (D^e/D^\infty - 1)/\phi_p$ versus the scaled polymer correlation length ξ/a, with $\upsilon_m^* = \gamma\upsilon_m/\upsilon_0 = 0.1$, 0.2, 0.4, and 1.0 (increasing upward) and $\phi^* = 0.8$ (solid lines). The dashed lines are exact solutions for impenetrable inclusions with a uniform coating of thickness ξ where $D(a < r < a + \xi) = D^\infty \exp(4\upsilon_m^*)$.

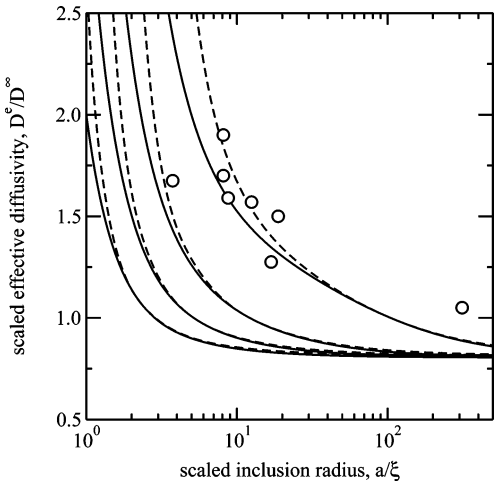

Figure 4. The scaled effective diffusivity D^e/D^∞ versus the scaled inclusion radius a/ξ, with $\upsilon_m^* = \gamma\upsilon_m/\upsilon_0 = 0.1$, 0.2, 0.4, and 1.0 (increasing upward), $\phi^* = 0.8$, and $\phi_p = 0.13$: $O(\phi_p)$ (solid lines) and $O(\phi_p^2)$ (dashed lines). The circles are experimental measurements of the permeability enhancement (from Merkel et al.[1] with their reported radii scaled using $\xi = 0.8$ nm).

is diminished (as in Maxwell's theory) because of the impenetrability of the inclusions. Also, because the relative increase in diffusivity depends exponentially on the penetrant size (eq 9), situations with multiple penetrants exhibit reverse selectivity,[1] as shown in the next subsection.

The diffusivity increment, defined as

$$\Delta = -3B/a^3 = (D^e/D^\infty - 1)/\phi_p + O(\phi_p) \qquad (32)$$

is plotted in Figure 3 as a function of ξ/a for various values of υ_m^* (solid lines). These calculations are compared with an exact solution for an impenetrable sphere with a uniform coating (see Appendix B) where the penetrant diffusivity equals the value given by eq 9 (dashed lines). Clearly, the effective diffusivity from eq 3 is much more sensitive to the layer characteristics, particularly when the layers are thick ($\xi/a > 1$).

To compare the theory with experiments, Figures 4 and 5 show the (scaled) effective diffusivity D^e/D^∞ and measured values of the (scaled) permeability (circles) for $\phi_p = 0.13$. The $O(\phi_p)$ theory (solid lines) neglects particle interactions, so the

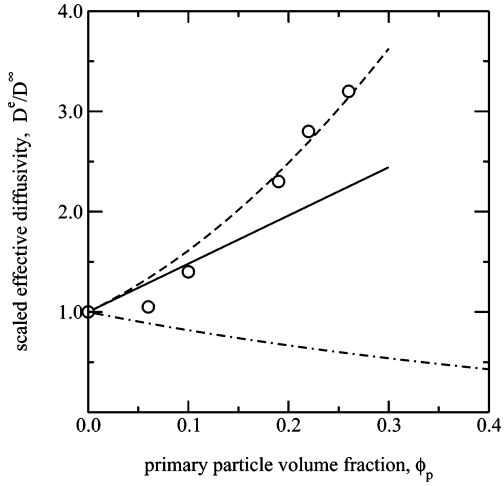

Figure 5. The scaled effective diffusivity D^e/D^∞ versus the inclusion volume fraction ϕ_p, with $\upsilon_m^* = \gamma\upsilon_m/\upsilon_0 = 1.0$, $\phi^* = 0.8$, and $\xi/a = 0.8/6.5 \approx 0.123$: exact $O(\phi_p)$ theory (solid line) and approximate $O(\phi_p^2)$ theory (dashed line). The circles are experimental measurements of the permeability enhancement (from Merkel et al.[1] with $a = 6.5$ nm). The dash−dotted line is Maxwell's self-consistent theory for impenetrable inclusions and unperturbed (homogeneous) polymer.

values are as given by eq 14. The dashed lines are the $O(\phi_p^2)$ theory (eq 22), which has elements of a self-consistent mean-field approximation with an explicit correction for interactions between pairs of particles in a statistically homogeneous dispersion.[11] Note that both the (single-particle) dipole strength and the particle concentration affect two-body interactions.

Some of the experimental scatter in Figure 4 may be attributed to the variety of filler particles (all embedded in PMP) and degrees of particle aggregation.[1] Nevertheless, with the foregoing approximations, the correlation length inferred by the fit is $\xi = 0.8$ nm (with $\phi^* = 0.8$) and, hence, the segment length $l \approx \sqrt{3}\xi \approx 1.4$ nm. The repeating unit of PMP comprises two bond lengths, so there are ~4.5 monomer units per statistical segment (in the immobilized and compressed chains). As expected, more flexible polymers in solution (e.g., poly(oxyethylene)) have much fewer (~2) repeat units per statistical segment (ref 12, p 168).

Figure 5 shows how the effective diffusivity (with $a = 6.5$ nm) increases with the inclusion volume fraction. The theory is presented with a correlation length $\xi = 0.8$ nm, which was obtained by fitting the model to the data in Figure 4, so $\xi/a = 0.8/6.5 \approx 0.123$. Despite the experiments extrapolating to a value of $D^e < D^\infty$ as $\phi_p \to 0$, the theoretical and experimental trends are in good agreement. For reference, the dash−dotted line is Maxwell's self-consistent theory

$$D^e/D^\infty = (1 - \phi_p)/(1 + \phi_p/2) \qquad (33)$$

for impenetrable inclusions in an unperturbed polymer matrix. It is remarkable, perhaps, that a perturbation extending only $\xi \approx 0.8$ nm from the inclusion surfaces can have such a significant influence on the bulk permeability. The next subsection quantifies Merkel et al.'s proposition that reverse selectivity arises from Cohen and Turnbull's free-volume theory.

3.2. Selectivity. If the penetrant solubility is independent of the inclusions, which, following the discussion of Merkel et al.'s data in the Introduction, is a reasonable approximation for certain solutes in PMP/fumed silica composites, then the influence of the inclusions on the experimentally measured selectivity α_{12} (eq 29) may be attributed entirely to the diffusive selectivity α_{12}^* (eq 30). It is then expedient to compare the

Table 1. Effective Diffusivity D^e/D^∞ (Scaled) and (Scaled) Diffusivity Selectivity $\alpha^*_{12}(\phi_p)/\alpha^*_{12}(0)$ as Functions of the Inclusion Volume Fraction ϕ_p and (Scaled) Penetrant Size υ^*_m ($\phi^* = 0.8$ and $\xi/a = 0.8/6.5$)[a]

ϕ_p	υ^*_m	D^e/D^∞ $O(\phi_p)$	D^e/D^∞ $O(\phi_p^2)$	$\alpha^*_{12}(\phi_p)/\alpha^*_{12}(0)$ $O(\phi_p^2)$
0.05	0.20	0.97	0.97	1.42
0.15	0.20	0.91	0.92	2.74
0.25	0.20	0.85	0.86	4.81
0.35	0.20	0.80	0.81	7.76
0.45	0.20	0.74	0.76	11.75
0.55	0.20	0.68	0.71	16.95
0.05	0.40	1.03	1.03	1.33
0.15	0.40	1.10	1.10	2.27
0.25	0.40	1.17	1.18	3.52
0.35	0.40	1.23	1.25	5.02
0.45	0.40	1.30	1.33	6.71
0.55	0.40	1.36	1.41	8.55
0.05	0.60	1.11	1.11	1.24
0.15	0.60	1.32	1.36	1.84
0.25	0.60	1.53	1.66	2.50
0.35	0.60	1.75	1.99	3.16
0.45	0.60	1.96	2.36	3.78
0.55	0.60	2.17	2.77	4.35
0.05	0.80	1.18	1.20	1.15
0.15	0.80	1.54	1.69	1.49
0.25	0.80	1.90	2.31	1.79
0.35	0.80	2.26	3.06	2.05
0.45	0.80	2.62	3.94	2.26
0.55	0.80	2.98	4.96	2.43
0.05	1.00	1.24	1.27	1.08
0.15	1.00	1.72	2.02	1.24
0.25	1.00	2.20	3.02	1.37
0.35	1.00	2.68	4.29	1.46
0.45	1.00	3.16	5.83	1.53
0.55	1.00	3.64	7.62	1.58
0.05	1.20	1.28	1.33	1.03
0.15	1.20	1.85	2.30	1.09
0.25	1.20	2.42	3.66	1.13
0.35	1.20	2.99	5.41	1.16
0.45	1.20	3.56	7.57	1.18
0.55	1.20	4.13	10.11	1.19
0.05	1.40	1.31	1.38	1.00
0.15	1.40	1.94	2.51	1.00
0.25	1.40	2.57	4.14	1.00
0.35	1.40	3.20	6.28	1.00
0.45	1.40	3.82	8.92	1.00
0.55	1.40	4.45	12.07	1.00

[a] In all cases, $\alpha^*_{12}(\phi_p)/\alpha^*_{12}(0)$ is calculated with $\upsilon^*_{m,1} = 1.4$. Selected data are plotted in Figure 6.

experimentally measured ratio $\alpha_{12}(\phi_p)/\alpha_{12}(0)$ with the theoretical value

$$\alpha^*_{12}(\phi_p)/\alpha^*_{12}(0) = \frac{D_1^e/D_1^\infty}{D_2^e/D_2^\infty} = \frac{1 - 3(B_1/a^3)\phi_p + 3(B_1/a^3)^2(1 - 0.44B_1/a^3)\phi_p^2 + ...}{1 - 3(B_2/a^3)\phi_p + 3(B_2/a^3)^2(1 - 0.44B_2/a^3)\phi_p^2 + ...} \quad (34)$$

Parameters that influence the (scaled) selectivity are $\upsilon^*_{m,1} = \gamma_1\upsilon_{m,1}/\upsilon_0$ and $\upsilon^*_{m,2} = \gamma_2\upsilon_{m,2}/\upsilon_0$, which, recall, reflect the size υ_m and shape γ of the molecules relative to the free-volume elements of the polymer matrix υ_0.

Table 1 lists representative values of the effective diffusivity D^e/D^∞ for (noninteracting) penetrants, which are distinguished only by υ^*_m (column 2). All calculations were performed with $\xi/a = 0.8/6.5$ and $\phi^* = 0.8$, so the results reflect changes in the size of the penetrant and the inclusion volume fraction. The membrane (diffusive) selectivity α^*_{12} (last column) is obtained from the $O(\phi_p^2)$ values of the effective diffusivity (fourth column). Note also that species 1 has $\upsilon^*_{m,1} = 1.4$; this provides reasonable values for the permeability enhancement of *n*-butane in PMP/fumed silica membranes. Since $\alpha_{12}(\phi_p) > \alpha^*_{12}(0)$, the selectivity to this (large) species is enhanced by inclusions. Clearly, these membranes exhibit reverse (diffusive) selectivity, with the permeability and selectivity to the larger species both increasing with the inclusion volume fraction and penetrant-size ratio.

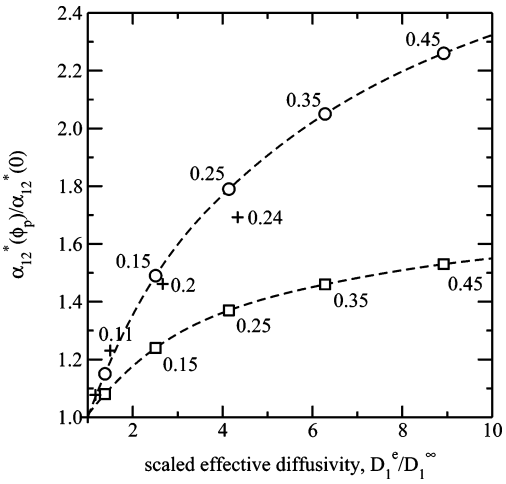

Figure 6. The (scaled) selectivity $\alpha^*_{12}(\phi_p)/\alpha^*_{12}(0)$ (eq 34) versus the scaled effective diffusivity D_1^e/D_1^∞ for various inclusion volume fractions $\phi_p = 0.05$, 0.15, 0.25, and 0.35 (values noted on the graph interpolated with dashed lines): $\phi^* = 0.8$; $\upsilon^*_{m,1} = 1.4$; $\upsilon^*_{m,2} = 0.8$ (circles) and 1.0 (squares). The crosses are the (scaled) selectivity $\alpha_{12}(\phi_p)/\alpha_{12}(0)$ for *n*-butane and methane in PMP/fumed silica membranes versus the relative permeability $P_1(\phi_p)/P_1(0)$ of *n*-butane (from Merkel et al.[1] Figure 2): $\phi_p = 0.063$, 0.11, 0.20, and 0.24.

To draw a closer connection to experiments, the diffusive selectivity $\alpha^*_{12}(\phi_p)/\alpha^*_{12}(0)$ is plotted in Figure 6 as a function of the effective diffusivity D_1^e/D_1^∞ for various inclusion volume fractions and two values of $\upsilon^*_{m,2}/\upsilon^*_{m,1} = 0.8/1.4 \approx 0.57$ (circles) and $1/1.4 \approx 0.71$ (squares). The theory is compared with experimentally measured values of the selectivity $\alpha_{12}(\phi_p)/\alpha_{12}(0)$ and permeability (crosses), as reported by Merkel et al.[1] (Figure 2) for *n*-butane (species 1) and methane (species 2) in PMP/fumed silica membranes. In both cases, the ordinate and abscissa are scaled with the respective values for membranes without inclusions. Note that the effective size ratio of methane and *n*-butane inferred by the theory is $\sim 0.8/1.4 \approx 0.57$. This is approximately 50% larger than the value $5/14 \approx 0.36$ expected from consideration of the atomic volume. As expected, the shape factor γ in $\upsilon^*_m = \gamma\upsilon_m/\upsilon_0$ reflects the molecular architecture. Accordingly, *n*-butane has a smaller effective volume per atom than methane. Despite the simplicity of the theoretical model, it is encouraging to see that it captures (almost quantitatively) the correct dependence of both the selectivity and the permeability on the inclusion volume fraction.

4. Summary

A theory has been developed to quantitatively interpret Merkel et al.'s experiments, which show that impenetrable nanoparticles embedded in permeable polymeric glasses increase gas permeability and selectivity. As proposed by Merkel et al., reverse diffusive selectivity emerges from Cohen and Turnbull's free-volume theory, which links polymer density to solute diffusivity. As shown in Figures 4 and 5, the model captures the correct dependence of the bulk permeability on particle size and volume fraction. Furthermore, Figure 6 demonstrates that this model also captures the correct (reverse) selectivity−

permeability relationship. It is noteworthy that the thickness of the polymer depletion layer ($\sim 1.5\xi = 1.2$ nm), established by fitting the transport model to measurements of the permeability enhancement, is the same as the diameter of the large free-volume elements ascertained by PALS (1.1−1.2 nm).

Note that theoretical predictions of the effective solute diffusivity have been compared with experimental measurements of the permeability enhancement. Therefore, the solubility was assumed to be independent of the inclusion concentration. Further, a mean-field description of the polymer segment density was adopted, with a flat, repulsive interface where the segment concentration vanishes. Also, the diffusion coefficient was assumed to follow Cohen and Turnbull's formula (eq 3), with the occupied volume being proportional to the atomic number density. Finally, theoretical predictions were based on a statistically homogeneous dispersion of inclusions, whereas the particles are often found to aggregate.

It remains to be established whether the enhanced (penetrant) diffusivity could also be due to enhanced segment mobility, as evidenced by rubbery interfaces that can coexist with a glassy bulk.[8] Further model development may also be required to quantify how penetrant solubility influences permeability and selectivity.

Nevertheless, despite the foregoing approximations, the semiquantitative agreement of theory and experiment provides a surprisingly simple and apparently robust interpretation of enhanced permeability and reverse selectivity in PMP/silica nanocomposite membranes.

Acknowledgment

Thiw work was supported by the Natural Sciences and Engineering Research Council of Canada (NSERC), through Grant No. 204542, and the Canada Research Chairs program (Tier II). The author is grateful to M. Maric (McGill University), for helpful discussions related to this work, and to three anonymous referees for valuable suggestions.

A Calculation of the Effective Diffusivity

Equation 14 is derived as follows. Adding and subtracting the flux $-D^\infty\nabla n$ from the integrand in eq 10 permits the average flux to be written as the sum of the flux in a homogeneous polymer matrix where $D = D^\infty$ and terms that account for the disturbances of the inclusions, i.e.,

$$\langle \mathbf{j}\rangle = -D^\infty V^{-1}\int_V \nabla n\,\mathrm{d}V - V^{-1}\int_V (D - D^\infty)\nabla n\,\mathrm{d}V$$
$$= -D^\infty\langle\nabla n\rangle - V^{-1}\int_V (D - D^\infty)\nabla n\,\mathrm{d}V \quad (35)$$

For well-dispersed particles, the integrand of the second integral on the right-hand-side of eq 35 vanishes beyond an $O(a + \xi)$ radial distance from the center of each inclusion. Therefore, the integral may be replaced by $N = n_\mathrm{p}V$ integrals (n_p is the inclusion number density) enclosing each inclusion and its layer of perturbed polymer. Then, neglecting particle interactions—assuming the inclusions are dispersed with uniform probability and small volume fraction—permits the N integrals to be replaced by N times the integral over a volume V_1 associated with a single inclusion in an unbounded polymer matrix, i.e.,

$$V^{-1}\int_V (D - D^\infty)\nabla n\,\mathrm{d}V = V^{-1}\sum_{i=1}^{N}\int_{V_i}(D - D^\infty)\nabla n\,\mathrm{d}V$$
$$\approx n_\mathrm{p}\int_{V_1}(D - D^\infty)\nabla n\,\mathrm{d}V \quad (36)$$

so

$$\langle \mathbf{j}\rangle \approx -D^\infty\langle\nabla n\rangle - n_\mathrm{p}\int_{V_1}(D - D^\infty)\nabla n\,\mathrm{d}V \quad (37)$$

When the continuous phase (polymer) is uniform, only the interior of the inclusions where $D = D^\mathrm{d}$ ($\neq D^\infty$) contributes to the integral in eq 37. However, with an inhomogeneous polymer, it is expedient to convert the volume integral to a distant surface integral. This is accomplished by splitting the volume integral into one over the interior ($r < a$) and another over the exterior ($a < r < \infty$).

When the diffusion coefficient inside the inclusion D^d is uniform, applying Gauss's integral theorem gives

$$n_\mathrm{p}\int_{r<a}(D - D^\infty)\nabla n\,\mathrm{d}V = n_\mathrm{p}(D^\mathrm{d} - D^\infty)\int_{r=a} n\hat{\mathbf{n}}\,\mathrm{d}A \quad (38)$$

where $\hat{\mathbf{n}}$ is an outward unit normal.

Outside the inclusion, it is necessary to apply the identity

$$\int \boldsymbol{\alpha}\,\mathrm{d}V = \int \mathbf{x}\boldsymbol{\alpha}\cdot\hat{\mathbf{n}}\,\mathrm{d}A - \int \mathbf{x}\nabla\cdot\boldsymbol{\alpha}\,\mathrm{d}V \quad (39)$$

where $\boldsymbol{\alpha}$ is an arbitrary vector field. Setting $\boldsymbol{\alpha} = (D - D^\infty)\nabla n = -\mathbf{j} - D^\infty\nabla n$ and noting that $\nabla\cdot\mathbf{j} = 0$ gives

$$n_\mathrm{p}\int_{r>a}(D - D^\infty)\nabla n\,\mathrm{d}V$$
$$= -n_\mathrm{p}\int_{r>a}\mathbf{j}\,\mathrm{d}V - n_\mathrm{p}D^\infty\int_{r>a}\nabla n\,\mathrm{d}V$$
$$= n_\mathrm{p}\int_{r=a}\mathbf{x}\mathbf{j}\cdot\hat{\mathbf{n}}\,\mathrm{d}A - n_\mathrm{p}\int_{r\to\infty}\mathbf{x}\mathbf{j}\cdot\hat{\mathbf{n}}\,\mathrm{d}A +$$
$$n_\mathrm{p}D^\infty\int_{r=a} n\hat{\mathbf{n}}\,\mathrm{d}A - n_\mathrm{p}D^\infty\int_{r\to\infty} n\hat{\mathbf{n}}\,\mathrm{d}A \quad (40)$$

Therefore, combining eqs 38 and 40 gives

$$n_\mathrm{p}\int_{V_i}(D - D^\infty)\nabla n\,\mathrm{d}V = n_\mathrm{p}D^\mathrm{d}\int_{r>a} n\hat{\mathbf{n}}\,\mathrm{d}A + n_\mathrm{p}\int_{r>a}\mathbf{x}\mathbf{j}\cdot\hat{\mathbf{n}}\,\mathrm{d}A -$$
$$n_\mathrm{p}\int_{r\to\infty}\mathbf{x}\mathbf{j}\cdot\hat{\mathbf{n}}\,\mathrm{d}A - n_\mathrm{p}D^\infty\int_{r\to\infty} n\hat{\mathbf{n}}\,\mathrm{d}A \quad (41)$$

which, because n and $\mathbf{j}$ are continuous and $D \to D^\infty$ as $r \to \infty$, can be written

$$n_\mathrm{p}\int_{V_1}(D - D^\infty)\nabla n\,\mathrm{d}V = n_\mathrm{p}D^\mathrm{d}\int_{r=a<}[n\hat{\mathbf{n}} - \mathbf{x}(\nabla n\cdot\hat{\mathbf{n}})]\,\mathrm{d}A -$$
$$n_\mathrm{p}D^\infty\int_{r\to\infty}[n\hat{\mathbf{n}} - \mathbf{x}(\nabla n\cdot\hat{\mathbf{n}})]\,\mathrm{d}A \quad (42)$$

where the subscript "$r = a <$" denotes that the gradient is to be evaluated "on the inclusion side of the interface at $r = a$ where $D = D^\mathrm{d}$".

Finally, the symmetries of the single-particle problem necessitate that the first surface integral in eq 42 vanishes, so

$$\langle \mathbf{j}\rangle \approx -D^\infty\langle\nabla n\rangle + n_\mathrm{p}D^\infty\int_{r\to\infty}[n\hat{\mathbf{n}} - \mathbf{x}(\nabla n\cdot\hat{\mathbf{n}})]\,\mathrm{d}A \quad (43)$$

Next, since the single-particle problem yields a far-field concentration

$$n \to \langle\nabla n\rangle\cdot\mathbf{r} + B\langle\nabla n\rangle\mathbf{r}/r^3 \text{ as } r \to \infty \quad (44)$$

where the scalar coefficient B is termed the *dipole strength*, evaluating the integral in eq 43 over the surface of a large concentric sphere yields

$$\langle \mathbf{j}\rangle \approx -D^\infty\langle\nabla n\rangle + 3\phi_\mathrm{p}(B/a^3)D^\infty\langle\nabla n\rangle + O(\phi_\mathrm{p}^2) \quad (45)$$

where $\phi_p = n_p(4/3)\pi a^3$ is the particle volume fraction and $\langle \nabla n \rangle$ is the average penetrant concentration gradient.

Under steady conditions, the penetrant concentration for a single spherical inclusion in an unbounded polymer has the form[13,14]

$$n = \text{const.} + \langle \nabla n \rangle \cdot \mathbf{r} + \langle \nabla n \rangle \cdot \mathbf{e}_r \hat{n}(r) \tag{46}$$

where $\mathbf{e}_r = \mathbf{r}/r$. Further, setting $\langle \nabla n \rangle = |\langle \nabla n \rangle| \mathbf{e}_z$, where $\mathbf{e}_z$ is the polar axis of a spherical coordinate system (r, θ, ϕ), gives

$$n = \text{const.} + |\langle \nabla n \rangle| r \cos\theta + |\langle \nabla n \rangle| \hat{n}(r) \cos\theta \tag{47}$$

where $\cos\theta = \mathbf{e}_r \cdot \mathbf{e}_z$. Finally, substituting eq 47 into the steady diffusion equation gives

$$\hat{n}_{rr} + (2/r)\hat{n}_r - (2/r^2)\hat{n} + (1 + \hat{n}_r) D_r/D = 0 \tag{48}$$

where subscripts indicate differentiation with respect to r, with boundary conditions

$$\hat{n}_r = -1 \text{ at } r = a \ (\mathbf{j} \cdot \hat{\mathbf{n}} = 0 \text{ when } D^d = 0) \tag{49}$$

and

$$\hat{n} \to B/r^2 \text{ as } r \to \infty \text{ (source dipole)} \tag{50}$$

In this work, B is obtained from an efficient numerical solution of eq 48.[13,14] For future reference, and to provide a convenient check on the numerical algorithm, Appendix B presents an analytical solution for penetrable inclusions ($D = D^d$) enveloped by a uniform concentric shell ($D = D^s$). The dipole strength is shown to be

$$B = a^3(1 + \xi/a)^3 \frac{(1 - D^s/D^\infty)[1 + (1 + \xi/a)^3(2 + D^d/D^s)/(1 - D^d/D^s)] + 3D^s/D^\infty}{(2 + D^s/D^\infty)[1 + (1 + \xi/a)^3(2 + D^d/D^s)/(1 - D^d/D^s)] - 3D^s/D^\infty} \tag{51}$$

where a is the radius of the primary particle and ξ is the thickness of the shell.

B. Diffusion Past a Composite Sphere

Equation 51 is derived as follows. A sphere with radius a_1 is centered at the origin ($r = 0$) of a spherical coordinate system. Inside the sphere ($r < a_1$), the penetrant diffusivity is D_1. The sphere is enveloped by a concentric shell with outer radius a_2 where the penetrant diffusivity is D_2. Beyond the shell ($r > a_2$), the penetrant diffusivity is D_3. The penetrant concentration n and flux $\mathbf{j} = -D_j \nabla n$ ($j = 1, 2, 3$) are continuous everywhere, and $n \to \text{const.} + \langle \nabla n \rangle \cdot \mathbf{r} + O(r^{-2})$ as $r \to \infty$.

The general solutions of Laplace's equation that satisfy the boundary conditions, symmetries, and linearity with respect to $\langle \nabla n \rangle$ are as follows:

$$n = c_0 - c_1 \langle \nabla n \rangle \cdot \mathbf{r} \quad (r < a_1) \tag{52}$$

$$n = c_2 - c_3 \langle \nabla n \rangle \cdot \mathbf{r} + c_4/r + c_5 \langle \nabla n \rangle \cdot \mathbf{r}/r^3 \quad (a_1 < r < a_2) \tag{53}$$

$$n = c_6 - c_7 \langle \nabla n \rangle \cdot \mathbf{r} + c_8/r + c_9 \langle \nabla n \rangle \cdot \mathbf{r}/r^3 \quad (r > a_2) \tag{54}$$

The 10 scalar coefficients $c_0, \ldots, c_9$ must be determined to satisfy the boundary conditions.

The two decaying terms that correspond to point sources (i.e., decaying as r^{-1}) vanish, so $c_4 = c_8 = 0$. Further, the far-field boundary condition requires $c_7 = -1$, and the boundary conditions must be independent of the addition of an arbitrary constant, so $c_0 = c_2 = c_6 = \text{const.}$ The remaining (interfacial) boundary conditions yield the coefficients of the two dipolar (i.e., decaying as r^{-2}) terms,

$$c_9 = a_2^3 \frac{(1 - D_2/D_3)[1 + (a_2/a_1)^3(2 + D_1/D_2)/(1 - D_1/D_2)] + 3D_2/D_3}{(2 + D_2/D_3)[1 + (a_2/a_1)^3(2 + D_1/D_2)/(1 - D_1/D_2)] - 3D_2/D_3} \tag{55}$$

and

$$c_5 = \frac{a_2^3 + c_9}{(a_2/a_1)^3(2 + D_1/D_2)/(1 - D_1/D_2) + 1} \tag{56}$$

and the coefficients of the remaining two linear (i.e., growing as r) terms:

$$c_3 = (c_5 - c_9)/a_2^3 - 1 \quad \text{and } c_1 = c_3 - c_5/a_1^3 \tag{57}$$

As shown in the main text, the effective diffusivity of a dilute composite can be written in terms of the dipole strength B ($=c_9$). It follows that the diffusivity increment is

$$\Delta \equiv (D^e/D_3 - 1)/\phi_p = -3B/a_1^3 = -3(a_2/a_1)^3 \frac{(1 - D_2/D_3)[1 + (a_2/a_1)^3(2 + D_1/D_2)/(1 - D_1/D_2)] + 3D_2/D_3}{(2 + D_2/D_3)[1 + (a_2/a_1)^3(2 + D_1/D_2)/(1 - D_1/D_2)] - 3D_2/D_3} \tag{58}$$

where $\phi_p = n_p(4/3)\pi a_1^3$ is the primary particle volume fraction.

The following limiting cases are summarized for convenient reference. Note that penetrant diffusion in this model is formally equivalent to heat or electrical conduction when the diffusivities are replaced by thermal or electrical conductivities; this is because the penetrant concentration is assumed to vary continuously across the interfaces.

"Infinitely Conductive" Shell: $D_2 \to \infty$. The composite sphere behaves as an infinitely conductive sphere with radius a_2:

$$\Delta \to 3(a_2/a_1)^3 \tag{59}$$

"Nonconductive" Shell: $D_2 \to 0$. The composite sphere behaves as a nonconductive sphere with radius a_2:

$$\Delta \to -(3/2)(a_2/a_1)^3 \tag{60}$$

Very Thick Shell: $a_2/a_1 \to \infty$. The composite sphere behaves as a homogeneous sphere with radius a_2, where the diffusivity is D_2:

$$\Delta \to -3(a_2/a_1)^3 \frac{(1 - D_2/D_3)}{(2 + D_2/D_3)} \tag{61}$$

Very Thin Shell: $a_2 \to a_1(1 + \epsilon)$ with $\epsilon \ll 1$.

$$\Delta \to -3\frac{(1 - D_2/D_3)(1 + 3\epsilon)(2 + D_1/D_2)/(1 - D_1/D_2) + 1 + 2D_2/D_3}{(2 + D_2/D_3)(1 + 3\epsilon)(2 + D_1/D_2)/(1 - D_1/D_2) + 2 - 2D_2/D_3} \tag{62}$$

Literature Cited

(1) Merkel, T. C.; Freeman, B. D.; Spontak, R. J.; He, Z.; Pinnau, I.; Meakin, P.; Hill, A. J. Ultrapermeable, reverse-selective nanocomposite membranes. *Science* **2002**, *296*, 519−522.

(2) Merkel, T. C.; Freeman, B. D.; Spontak, R. J.; He, Z.; Pinnau, I.; Meakin, P.; Hill, A. J. Sorption, transport, and structural evidence for enhanced free volume in poly(4-methyl-2-pentyne)/fumed silica nanocomposite membranes. *Chem. Mater.* **2003**, *15*, 109−123.

(3) Merkel, T. C.; Toy, L. G.; Andrady, A. L.; Gracz, H.; Stejskal, E. O. Investigation of enhnaced free volume in nanosilica-filled poly(1-trimethylsilyl-1-propyne) by ^{129}Xe NMR spectroscopy. *Macromolecules* **2003**, *36*, 353−358.

(4) Gomes, D.; Nunes, S. P.; Peinemann, J.-V. Membranes for gas separation based on poly(1-trimethylsilyl-1-propyne)-silica nanocomposites. *J. Membr. Sci.* **2005**, *246*, 13−25.

(5) Winberg, P.; DeSitter, K.; Dotremont, C.; Mullens, S.; Vankelecom, I. F. J.; Maurer, F. H. J. Free volume and interstitial mesopores in silica filled poly(1-trimethlysilyl-1-propyne) nanocomposites. *Macromolecules* **2005**, *38*, 3776−3782.

(6) Zhong, J.; Lin, G.; Wen, W.-Y.; Jones, A. A.; Kelman, S.; Freeman, B. D. Translation and rotation of penetrants in [an] ultrapermeable nanocomposite membrane of poly(2,2-bis(trifluoromethyl)-4,5-difluoro-1,3-dixole-*co*-tetrafluoroethylene) and fumed silica. *Macromolecules* **2005**, *38*, 3754−3764.

(7) Cohen, M. H.; Turnbull, D. Molecular transport in liquids and glasses. *J. Chem. Phys.* **1959**, *31*, 1164−1169.

(8) Bansal, A.; Yang, H.; Li, C.; Cho, K.; Benicewicz, B. C.; Kumar, S. K.; Schadler, L. S. Quantitative equivalence between polymer nanocomposites and thin polymer films. *Nat. Mater.* **2005**, *4*, 693−698.

(9) Hervet, H.; Léger, L.; Rondelez, F. Self-diffusion in polymer solutions: A test for scaling and reptation. *Phys. Rev. Lett.* **1979**, *42*, 1681−1684.

(10) de Gennes, P. G. *Scaling Concepts in Polymer Physics*; Cornell University Press: Ithaca, NY, 1979.

(11) Jeffrey, D. J. Conduction through a random suspension of spheres. *Proc. R. Soc. London, Ser. A* **1973**, *335*, 355−367.

(12) Russel, W. B.; Saville, D. A.; Schowalter, W. R. *Colloidal Dispersions*; Cambridge University Press: Cambridge, 1989 (paperback edition, 1991).

(13) Hill, R. J.; Saville, D. A.; Russel, W. B. Electrophoresis of spherical polymer-coated colloidal particles. *J. Colloid Interface Sci.* **2003**, *258*, 56−74.

(14) Hill, R. J. Transport in polymer-gel composites: theoretical methodology and response to an electric field. *J. Fluid Mech.* **2006**, *551*, 405−433.

Received for review October 28, 2005
Revised manuscript received February 12, 2006
Accepted February 12, 2006

IE0512035